

Twin-Polaritons: Classical versus Quantum Features in Polaritonic Spectra

Irén Simkó^{1,2,*} and Norah M. Hoffmann^{1,2,3,†}

¹Department of Chemistry, New York University, New York, New York 10003, USA

²Simons Center for Computational Physical Chemistry at New York University, New York, New York 10003, USA

³Department of Physics, New York University, New York, New York 10003, USA

(Dated: March 26, 2025)

Understanding whether a polaritonic phenomenon is inherently quantum or classical is essential for developing accurate models and optimizing experimental designs. We investigate this question in the context of polaritonic rotational-vibrational spectra and report a new feature, the twin-polariton, an additional splitting beyond the usual primary resonant polariton splitting that arises from light-matter entanglement. Through *ab-initio* calculations of HCl molecules and a corresponding model system coupled to a cavity, we demonstrate that the twin-polariton persists in the many-molecule case and follows the same linear dependence on coupling strength as the primary resonant polariton splitting. This finding reveals a novel mechanism to tune a quantum feature using a classical one, offering new insights into the fundamental nature of polaritonic systems.

Strong light-matter coupling, achievable in optical or plasmonic cavities, forms hybrid light-matter states, called polaritons, and offers a novel and promising way to alter material properties and steer chemical reactions without an external driving field [1–5]. Due to its potential applications, including manipulating chemical reactivity [1], tuning exciton transport [6], and enabling room-temperature exciton-polariton condensation [7], the number of experimental [1, 4, 8–13] and theoretical [14–25] studies in molecular polaritonics has rapidly increased in recent years. However, a significant gap remains between experimental reality, which often requires many molecules for strong coupling, and theoretical models, which struggle with such large-scale calculations. Consequently, conflicting findings persist, highlighting the need for further experimental and theoretical study.

One key question that remains is: Which polaritonic phenomena can be fully explained through classical optics and which require a more advanced quantum theoretical framework? For instance, the main spectral signature of strong light-matter coupling, the polariton splitting, is often considered a classical feature and Ref. 26 indicates that many polaritonic phenomena can be explained by polaritons acting as classical optical filters in the $N_{\text{mol}} \rightarrow \infty$ limit. However, this classical filtering picture may break down [26] in cases such as polariton-assisted photon recycling [27], polaritonic 2D IR spectroscopy [28] and for systems with many quanta of excitation or few-molecule strong coupling. [26]

Understanding whether a polaritonic phenomenon is quantum or classical is crucial for developing accurate theoretical models, optimizing experimental designs, and resolving conflicting findings. In this paper, we explore this question in the context of molecular rotational-vibrational spectra. We investigate the role of treating the cavity mode classical or quantum mechanically coupled to a quantum molecular system and report an intriguing new feature of the polaritonic

spectrum that requires a quantum treatment of light and does not appear when calculated classically. We call this feature the Twin-Polariton (TP), an additional splitting beyond the primary resonant polariton splitting in the rotational-vibrational spectrum of gas-phase molecules coupled to the cavity mode. We investigate the TP for HCl molecules coupled to a cavity (calculated fully *ab-initio*), corroborate our findings with a tunable three-level model system, and explore the $N_{\text{mol}} \rightarrow \infty$ thermodynamic limit [29]. We show that the TP persists in the many-molecule case and that its description requires a quantum treatment of light due to light-matter entanglement. Most interestingly, the TP splitting appears in addition to the primary resonant polariton splitting and follows the same rule: a linear increase in splitting with coupling strength. This allows us to tune a quantum feature (i.e. the additional TP splitting) using a classical feature (i.e. the primary resonant polariton splitting).

We first define classical and quantum photon modes. A classical photon mode follows Maxwell’s equations with boundary conditions (e.g., cavity mirrors), leading to the discretization (or quantization) of light frequencies. However, quantized does not necessarily imply quantum. These modes represent discretized field distributions from boundary conditions but do not account for quantum phenomena such as vacuum field fluctuations or entanglement. In contrast, in the quantum treatment of light, each quantized photon mode is described by the $|N\rangle$ eigenstates of the photonic Hamiltonian (i.e., Fock states), corresponding to N photons with a specific frequency.

We consider a coupled light-matter system described by the non-relativistic Hamiltonian in the dipole approximation and Coulomb gauge [19, 30–34] (using atomic units throughout):

$$\hat{H} = \hat{H}_{\text{mol}} + \hat{H}_{\text{ph}} + g\sqrt{2\omega_c}\hat{q}(\hat{\boldsymbol{\mu}} \cdot \boldsymbol{\xi}) + \frac{g^2}{\omega_c}(\hat{\boldsymbol{\mu}} \cdot \boldsymbol{\xi})^2. \quad (1)$$

Here, \hat{H}_{mol} is the molecular Hamiltonian, and $\hat{H}_{\text{ph}} =$

$(\hat{p}^2 + \omega_c^2 \hat{q}^2)/2$ is the photonic Hamiltonian for a single photon mode with frequency ω_c . The coordinate \hat{q} denotes the photonic displacement-field, and \hat{p} represents the momentum. The last two terms of Eq. (1) describe the dipole interaction and the dipole self-energy, with dipole moment $\hat{\mu}$, polarization direction $\xi = Z$, and the coupling strength g .

In the **classical case**, $p(t)$ and $q(t)$ are scalar variables, and the polaritonic spectrum is obtained by time evolving the molecular state $|\Psi(t)\rangle$ and the photonic variables:

$$i\dot{|\Psi(t)\rangle} = -i\left(\hat{H}_{\text{mol}} + g\sqrt{2\omega_c}q(t)(\hat{\mu} \cdot \xi) + \frac{g^2}{\omega_c}(\hat{\mu} \cdot \xi)^2\right)|\Psi(t)\rangle \quad (2)$$

$$\dot{p}(t) = -\omega_c^2 q(t) - g\sqrt{2\omega_c} \langle \Psi(t) | \hat{\mu} \cdot \xi | \Psi(t) \rangle \quad (3)$$

and $\dot{q}(t) = p(t)$, where $|\Psi(t)\rangle$ is expressed in the $|\psi_n\rangle$ eigenstates of \hat{H}_{mol} . The initial conditions for the photonic vacuum state are $p(0) = q(0) = 0$, and the molecular initial state is given by $|\Psi(0)\rangle = |\psi_i\rangle$. We obtain the absorption spectrum by applying an initial kick and Fourier-transforming the dipole autocorrelation function (see SI II.A.). In the **quantum case**, \hat{q} and \hat{p} are expressed in terms of the creation \hat{a}^\dagger and annihilation \hat{a} operators, with the light-matter Hamiltonian taking the form:

$$\hat{H} = \hat{H}_{\text{mol}} + \omega_c \hat{a}^\dagger \hat{a} + g(\hat{a}^\dagger + \hat{a})(\hat{\mu} \cdot \xi) + \frac{g^2}{\omega_c}(\hat{\mu} \cdot \xi)^2. \quad (4)$$

The Hamiltonian matrix is constructed using the direct product basis of the molecular eigenstates $|\psi_n\rangle$ and the photonic number states $|N\rangle$. In the quantum case, we employ two approaches to obtain the spectrum (see SI II.B.). The first, commonly used, involves solving the static Schrödinger equation by diagonalizing the Hamiltonian to determine the polariton eigenstates. Alternatively, we calculate the spectrum using a time-dependent approach. In this method, we solve the time-dependent Schrödinger equation with the initial state $|\Psi(0)\rangle = |\psi_i, 0\rangle = |\psi_i\rangle |0\rangle$. As in the classical model, we apply a kick and obtain the spectrum from the dipole autocorrelation function. The latter approach is needed for direct comparison with the classical case and to determine time-dependent observables such as populations.

To investigate classical versus quantum features in polaritonic spectra, we examine the gas-phase infrared spectra of HCl molecules coupled to a cavity mode, at $T = 300\text{K}$ (see SI I.A. for molecular model). This system allows us to analyze individual rotational-vibrational transitions and their modifications under strong coupling. Our study is motivated by recent experiments reporting strong coupling features in gas-phase systems [11, 35, 36]. Figure 1(a) illustrates the rotational-vibrational states of the HCl molecule (left) coupled to a

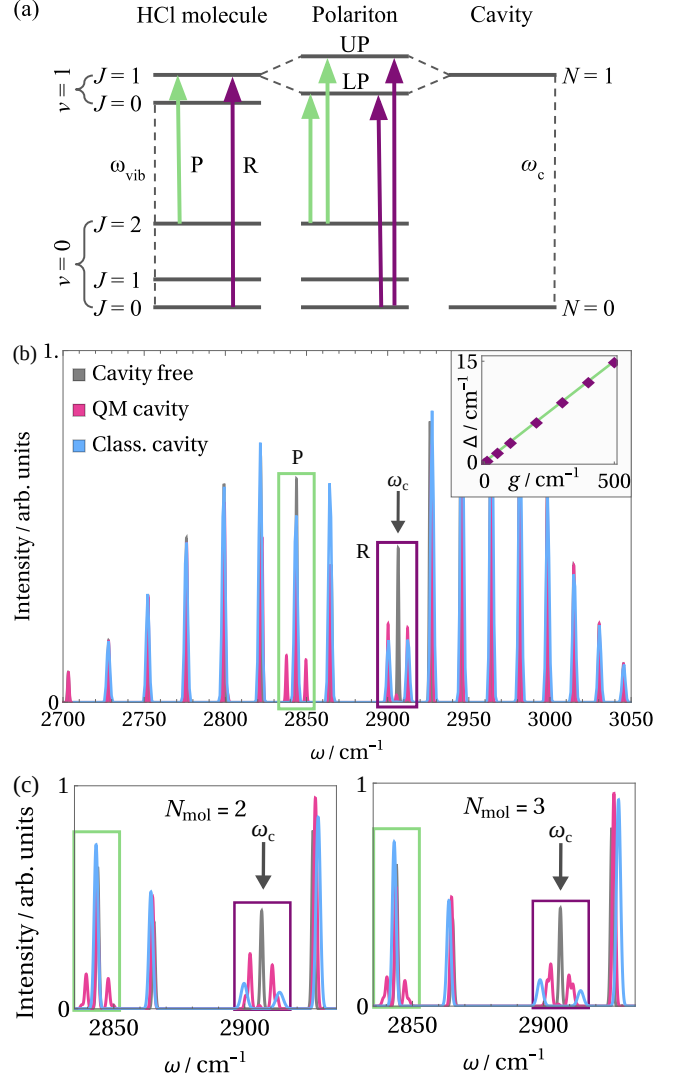


FIG. 1. (a) Energy-level diagram of a HCl molecule coupled to a cavity mode ω_c , with the R-branch (purple) and P-branch (green) transitions. (b) Polaritonic rovibrational spectrum of HCl at $T = 300\text{K}$, coupled to a cavity mode ($\omega_c = 2906.46\text{ cm}^{-1}$, arrow) with coupling strength $g = 400\text{ cm}^{-1}$, using the classical (blue) and quantum (pink) cavity models. The cavity-free spectrum is in gray. The inset shows the primary and twin-polariton splittings vs. coupling strength for the quantum case. (c) Polaritonic rovibrational spectrum for $N_{\text{mol}} = 2, 3$ HCl molecules with $g\sqrt{N_{\text{mol}}} = 400\text{ cm}^{-1}$, using the same parameters as (b).

cavity mode polarized in the Z -direction (right), which is resonant with the R -branch transition $|v, J, M\rangle = |0, 0, 0\rangle \rightarrow |1, 1, 0\rangle$. Here, v denotes the vibrational quantum number, and J, M are the rotational quantum numbers. This coupling results in a lower and upper polariton splitting (purple, middle). The corresponding spectrum is shown in Figure 1(b), where the cavity-free spectrum is plotted in gray, and the spectra for the quantum and classical cavity cases are plotted in pink and

blue, respectively. In the R -branch region (purple box, Fig. 1(b)), the polariton splitting is clearly observed in both the classical and quantum calculations, consistent with previous reports that the primary polariton splitting is a classical feature [26, 37].

The dipole selection rules $\Delta J = \pm 1$ and $\Delta M = 0$ for light polarized along Z allow an additional optically active transition $|v, J, M\rangle = |0, 2, 0\rangle \rightarrow |1, 1, 0\rangle$ in the P -branch (green, left and middle of Fig. 1(a)). This transition shares the same final state as the R -branch transition and hence also splits into the upper and lower polariton (green box, Fig. 1(b)). These TP peaks follow the same rule as the primary polariton splitting: the splitting increases linearly with the coupling strength. This is highlighted in the inset of Fig. 1(b), where the purple squares represent the Rabi splitting of the primary polariton and the green line represents that of the TP. This tunability allows the off-resonant TP features to be controlled via the primary resonant polariton. Note that there is also a central peak due to selection rules of the M quantum number. More precisely, in the polariton formation, the state has $J = 1$ with $M \in \{-1, 0, 1\}$, but only $M = 0$ can create polaritons. Specifically, $|v = 1, J = 1, M = 0\rangle |N = 0\rangle$ hybridizes with $|v = 0, J = 0, M = 0\rangle |N = 1\rangle$, while the other $|v = 1, J = 1, M = \pm 1\rangle |N = 0\rangle$ states remain unchanged (SI III.).

Although the TP phenomenon appears somewhat obvious, as this is true for all optically allowed transitions sharing the same final polariton states, its intriguing aspect lies in its quantum origin. Figure 1(b) (green box) shows that the TP appears only in the quantum calculation, while the spectrum remains unchanged from the cavity-free case in the classical calculation. This observation persists when the number of HCl molecules is increased to three (Fig. 1(c)). These findings raise two important questions: (i) Does this feature persist in the many-molecule case? (ii) Is this feature fundamentally quantum in nature, and if so, what defines its quantum character?

First, we investigate whether the TP persists in the **many-molecule limit**. (see SI II.D.). While our *ab-initio* calculations has been extended up to three HCl molecules and show that the feature persists as the number increases, this remains insufficient to represent an actual many-molecule regime. To overcome this limitation of few-molecule representation and to gain further physical insight, we employ a three-level model system that represents the rotational-vibrational states of the HCl molecule (Fig. 2(a)). Assuming thermal populations of E_0 and E_1 as $p_0 = p_1 = 0.5$, the 3-level model system exhibits two transitions at $8 \cdot 10^{-3}$ a.u. (P transition, green) and $10 \cdot 10^{-3}$ a.u. (R transition, purple). Figure 2(b) shows the corresponding cavity-free spectrum (gray) and the spectra when coupled to the cavity mode resonant with the R-branch transition, calculated

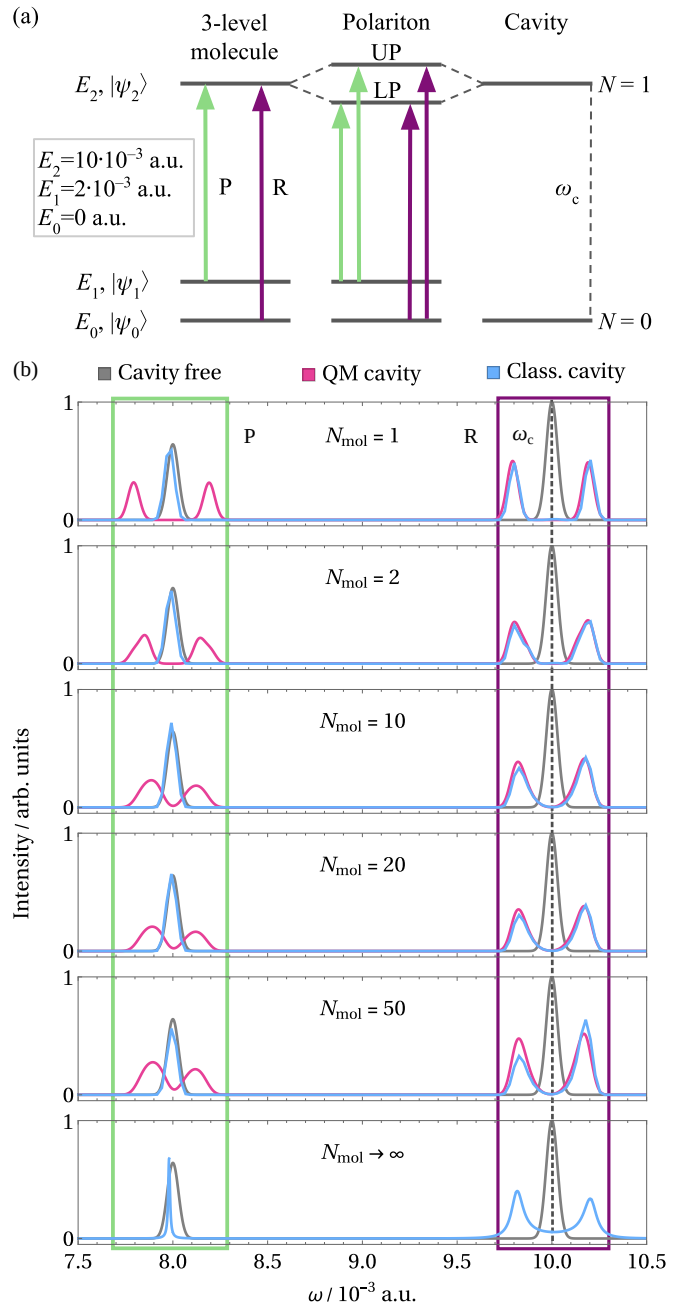


FIG. 2. (a) Energy-level diagram of the 3-level model system coupled to the cavity mode ω_c . (b) Polaritonic spectrum for increasing number of molecules top to bottom for $g\sqrt{N_{\text{mol}}} = 0.2 \cdot 10^{-3}$ a.u. and $\omega_c = 10 \cdot 10^{-3}$ a.u. (denoted by dashed line) obtained with the quantum (pink) and classical (blue) cavity models.

using classical (blue) and quantum (pink) light description. From top to bottom, we increase the number of molecules N_{mol} up to 50, with the coupling strength normalized by $\sqrt{N_{\text{mol}}}$. Since the system is in the gas phase, we neglect intermolecular interactions. However, we incorporate the Pauli principle, which is essential for few-molecule polaritonic states [38, 39]. Interestingly, we

find that the TP feature persists in the many-molecule regime and remains observable only in the quantum calculation. Note that both the primary and TP features converge at $N_{\text{mol}} = 10$, and the central TP peak, discussed for the HCl molecule, is absent since the M quantum number's degeneracy is not applicable.

Given that the *classical* calculation combines a classical treatment of light with a quantum description of the material, one might question whether the absence of the TP in the classical case arises from errors introduced by semiclassical assumptions. To resolve this, we analyze the spectrum using a fully classical model (Ref. 29), which avoids semiclassical artifacts and describes the $N_{\text{mol}} \rightarrow \infty$ limit (Fig. 2(b), bottom panel). In this model, the polaritonic absorption spectrum is obtained from the linear molecular susceptibility, $\chi(\omega)$, and rate of photon escape, κ :

$$I(\omega) = \frac{\frac{1}{2}\kappa\omega_c\text{Im}[\chi(\omega)]}{|\omega - \omega_c + i\frac{\kappa}{2} + \frac{\omega_c}{2}\chi(\omega)|^2} \quad (5)$$

(see also SI I. B.). Consistent with the case of 50 molecules, the $N_{\text{mol}} \rightarrow \infty$ classical spectrum shows no splitting for the P peak, confirming that the absence of the TP feature results from the classical treatment of light, rather than errors introduced by semiclassical methods.

Having confirmed that the TP feature persists in the many-molecule case, we now turn to the question of whether it constitutes an actual quantum effect and, if so, what defines its quantum character. To address this, we analyze the time-dependent population dynamics of our three-level system in both classical and quantum descriptions. In the classical case, the cavity coupled molecular wavefunction $|\Psi(t)\rangle$ is given by

$$|\Psi(t)\rangle = \sum_i C_{i,q}(t)e^{-iE_i t} |\psi_i\rangle, \quad (6)$$

and the corresponding population of the $|\psi_i\rangle$ state is $p_{i,q}(t) = |C_{i,q}(t)|^2$, where i denotes the molecular state and q accounts for the classical photon mode dependence of the wavefunction, obtained by solving Eqs.(2-3). In the quantum case, the wavefunction and its corresponding population are defined as

$$|\Psi(t)\rangle = \sum_N \sum_i C_{i,N}(t)e^{-i(E_i + N\omega_c)t} |\psi_i, N\rangle, \quad (7)$$

and $p_{i,N}(t) = |C_{i,N}(t)|^2$, where N denotes the photon Fock state. The time-dependent populations for both the classical and quantum cases are plotted in Fig. 3(a,b) respectively. Furthermore, the dipole moment can be expressed as

$$\mu(t) = \sum_N \sum_{i,j} C_{j,N}^*(t)C_{i,N}(t)e^{-i(E_i - E_j)t} \langle \psi_j | \hat{\mu} | \psi_i \rangle. \quad (8)$$

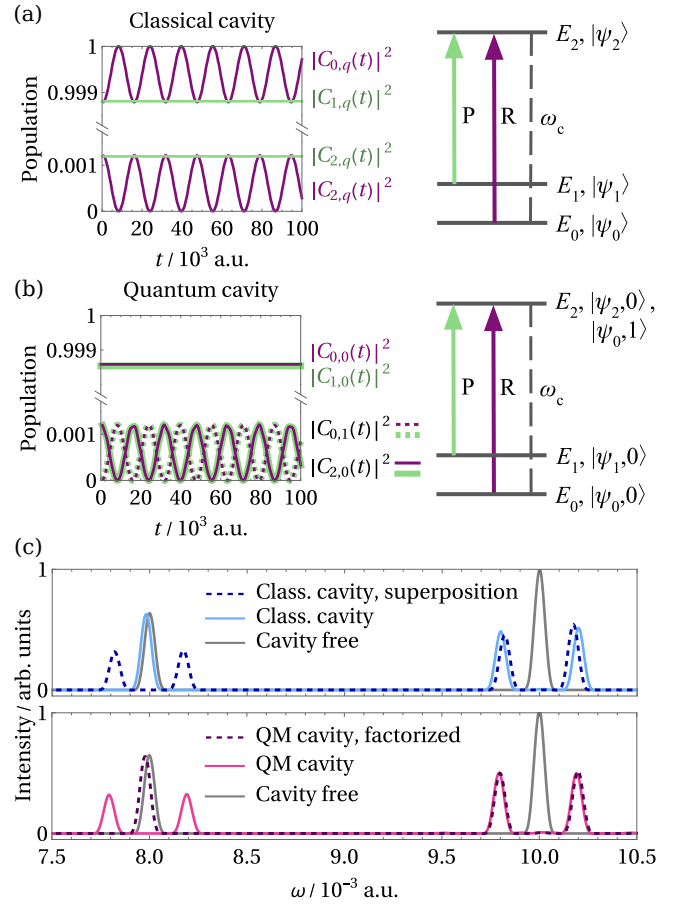


FIG. 3. (a-b) Population analysis for the time-dependent classical (a) and quantum (b) cavity simulations for R-branch (purple) and P-branch (green) transition with the same cavity parameters in Fig. 2. (c) Classical cavity simulation (light blue, solid) compared to the classical cavity simulation starting in a superposition initial state $|\Psi(0)\rangle = (|\psi_0\rangle + |\psi_1\rangle)/\sqrt{2}$ (blue, dashed), and quantum cavity simulation (pink, solid) compared to the quantum cavity simulation assuming factorized light-matter wave function (dark pink, dashed).

in the quantum case and as

$$\mu(t) = \sum_{i,j} C_{j,q}^*(t)C_{i,q}(t)e^{-i(E_i - E_j)t} \langle \psi_j | \hat{\mu} | \psi_i \rangle \quad (9)$$

in the classical case, where i, j denote molecular states. This establishes a direct connection between population transfer and spectral features via the Fourier transform of the time-dependent dipole moment.

In other words, an oscillatory population transfer with frequency Ω leads to a peak splitting with a separation of $\hbar\Omega$, whereas a constant population transfer results in a single peak.

Fig. 3(a) presents the classical population dynamics of the three-level system, where $|C_{(0,1,2),q}(t)|^2$ denote the populations of the respective states $E_{(0,1,2)}$, with the R-branch transition shown in purple and the P-branch

in green. In the classical case, we observe that only the R-branch transition exhibits oscillatory populations $|C_{0,q}(t)|^2$ and $|C_{2,q}(t)|^2$, indicating oscillatory energy transfer between the molecule and the cavity mode. The population oscillation results in the expected primary resonant polariton peak splitting due to cavity mode coupling. In contrast, for the P-branch, the populations $|C_{1,q}(t)|^2$ and $|C_{2,q}(t)|^2$ remain constant, explaining the absence of TP splitting in the classical calculation. Turning to the quantum case, depicted in Fig. 3(b), we find a striking difference: **both** the R-branch and P-branch transitions exhibit oscillatory populations $|C_{2,0}(t)|^2$ and $|C_{0,1}(t)|^2$ (corresponding to the $|\psi_{2,0}\rangle$ and $|\psi_{0,1}\rangle$ basis states). This oscillation ultimately gives rise to both the main and TP splittings. Thus, in the quantum case, the TP originates from the $|\psi_{0,1}\rangle$ and $|\psi_{2,0}\rangle$ degeneracy. In other words, the P-branch transition $|\psi_{1,0}\rangle \rightarrow |\psi_{2,0}\rangle$ must "know" that the photon mode couples to the $|\psi_{0,0}\rangle \rightarrow |\psi_{2,0}\rangle$ transition in order to induce the TP, which is encoded in the $|\psi_{0,1}\rangle$ state. This also explains why the TP is absent in the classical thermodynamic limit. Here the classical susceptibility function accounts only for transition frequencies and does not capture the shared final state of the P-branch and R-branch transitions.

To gain deeper insight into the quantum nature of the TP, we investigate the roles of key characteristics of quantum light: vacuum-field fluctuations, photon number states, and light-matter entanglement. In this context, light-matter entanglement refers to the situation in which the wavefunction of the coupled system cannot be factorized into independent photonic and molecular components, serving as a measure of non-classical correlations that cannot be captured by independent subsystem descriptions. To identify the quantum feature responsible for the TP, we simulate a time-dependent quantum system assuming a factorized light-matter wavefunction: $|\Psi(t)\rangle = (\sum_i a_i |\psi_i\rangle) (\sum_N b_N |N\rangle)$ (see also SI II.C.). This assumption includes vacuum-field fluctuations and photon number states but explicitly prevents light-matter entanglement due to the enforced factorization. Indeed, comparing the original quantum calculation (Fig. 3(c), pink) with the factorized case (dashed dark purple), we find the TP vanishes, indicating that light-matter entanglement, an intrinsically quantum characteristic, is essential.

Given this insight, we now ask how to modify the classical calculation to recover the TP feature. Since light-matter entanglement is key, we artificially introduce it by initializing the classical calculation in a superposition state $|\Psi(0)\rangle = (|\psi_0\rangle + |\psi_1\rangle)/\sqrt{2}$ rather than an eigenstate. While this does not reflect the physical system's true initial state, it serves to illustrate the role of entanglement. Indeed, when starting in a superposition state, implicitly including light-matter entanglement via population transfer to $|\psi_0\rangle$, we recover the TP

feature (Fig. 3(c) top panel, dashed dark blue), unlike when starting in a pure $|\psi_1\rangle$ state (Fig. 3(c), light blue).

In conclusion, we investigated classical versus quantum features in the polaritonic rotational-vibrational spectrum of gas-phase molecules. We identified an intriguing new feature: the Twin-Polariton (TP), arising from light-matter entanglement. Through *ab-initio* calculations of HCl molecules and model systems, we demonstrated its persistence in the many-molecule case. Remarkably, the TP appears alongside the primary resonant polariton splitting and follows the same linear dependence on coupling strength, allowing a quantum feature (the TP) to be tuned using a classical one (the primary resonant polariton splitting). Note, these twin-polaritons can also be induced in reverse: when the cavity mode is resonant with the P-branch transition, the TP can be observed in the R-branch, provided that the two transitions are optically allowed and share the same final state. This provides a novel lever for manipulating polaritonic systems and offers new insights into their fundamental nature. Finally, the TP is a previously unreported polaritonic phenomenon. Due to its off-resonant character, we hypothesize that experimental observation of the TP will require measuring the absorption spectrum through the non-confined direction of the cavity rather than via traditional transmission spectroscopy (SI III.) [11, 35, 36].

ACKNOWLEDGEMENTS

This work was supported by the Simons Center for Computational Physical Chemistry (SCCPC) at NYU (SF Grant No. 839534). Additional support was provided in part through NYU IT High Performance Computing resources, services, and staff expertise. Simulations were partially executed on resources supported by the SCCPC. I.S. acknowledges support from a postdoctoral fellowship awarded by the SCCPC at NYU.

* is2873@nyu.edu

† norah.hoffmann@nyu.edu

- [1] T. W. Ebbesen, *Acc. Chem. Res.* **49**, 2403 (2016).
- [2] F. Herrera and J. Owrutsky, *J. Chem. Phys.* **152**, 100902 (2020).
- [3] B. S. Simpkins, A. D. Dunkelberger, and J. C. Owrutsky, *J. Phys. Chem. C* **125**, 19081 (2021).
- [4] K. Nagarajan, A. Thomas, and T. W. Ebbesen, *J. Am. Chem. Soc.* **143**, 16877 (2021).
- [5] A. D. Dunkelberger, B. S. Simpkins, I. Vurgaftman, and J. C. Owrutsky, *Annu. Rev. Phys. Chem.* **73**, 429 (2022).
- [6] D. Xu, A. Mandal, J. M. Baxter, S.-W. Cheng, I. Lee, H. Su, S. Liu, D. R. Reichman, and M. Delor, *Nat. Commun.* **14**, 3881 (2023).

- [7] A. M. Berghuis, G. W. Castellanos, S. Murai, J. L. Pura, D. R. Abujetas, E. van Heijst, M. Ramezani, J. A. Sánchez-Gil, and J. G. Rivas, *Nano Lett.* **23**, 5603 (2023).
- [8] F. J. Garcia-Vidal, C. Ciuti, and T. W. Ebbesen, *Science* **373**, eabd0336 (2021).
- [9] B. Xiang and W. Xiong, *Chem. Rev.* **124**, 2512 (2024).
- [10] R. Bhuyan, J. Mony, O. Kotov, G. W. Castellanos, J. G. Rivas, T. O. Shegai, and K. Börjesson, *Chem. Rev.* **123**, 10877 (2023).
- [11] M. L. Weichman and J. C. Nelson, *J. Chem. Phys.* **161**, 074304 (2024).
- [12] K. Hirai, J. A. Hutchison, and H. Uji-i, *ChemPlusChem* **85**, 1981 (2020).
- [13] K. Hirai, J. A. Hutchison, and H. Uji-i, *Chem. Rev.* **123**, 8099 (2023).
- [14] J. Yuen-Zhou, W. Xiong, and T. Shegai, *J. Chem. Phys.* **156**, 034103 (2022).
- [15] M. Ruggenthaler, N. Tancogne-Dejean, J. Flick, H. Appel, and A. Rubio, *Nat. Rev. Chem.* **2**, 0118 (2018).
- [16] D. S. Wang and S. F. Yelin, *ACS Photonics* **8**, 2818 (2021).
- [17] J. Fregoni, F. J. Garcia-Vidal, and J. Feist, *ACS Photonics* **9**, 1096 (2022).
- [18] M. Sánchez-Barquilla, A. I. Fernández-Domínguez, J. Feist, and F. J. Garcia-Vidal, *ACS Photonics* **9**, 1830 (2022).
- [19] M. Ruggenthaler, N. Tancogne-Dejean, J. Flick, H. Appel, and A. Rubio, *Nat. Rev. Chem.* **2**, 0118 (2018).
- [20] J. Flick, N. Rivera, and P. Narang, *Nanophotonics* **7**, 1479 (2018).
- [21] D. Sidler, M. Ruggenthaler, C. Sch" afer, E. Ronca, and A. Rubio, *J. Chem. Phys.* **156**, 230901 (2022).
- [22] M. Ruggenthaler, D. Sidler, and A. Rubio, *Chem. Rev.* **123**, 11191 (2023).
- [23] A. Mandal, M. A. D. Taylor, B. M. Weight, E. R. Koessler, X. Li, and P. Huo, *Chem. Rev.* **123**, 9786 (2023).
- [24] R. F. Ribeiro, L. A. Martínez-Martínez, M. Du, J. Campos-Gonzalez-Angulo, and J. Yuen-Zhou, *Chem. Sci.* **9**, 6325 (2018).
- [25] T. E. Li, B. Cui, J. E. Subotnik, and A. Nitzan, *Annu. Rev. Phys. Chem.* **73**, 43 (2022).
- [26] K. Schwennicke, A. Koner, J. B. Pérez-Sánchez, W. Xiong, N. C. Giebink, M. L. Weichman, and J. Yuen-Zhou, *arXiv* (2024), 10.48550/arXiv.2408.05036.
- [27] J. B. Pérez-Sánchez and J. Yuen-Zhou, *arXiv* (2024), 10.48550/arXiv.2407.20594.
- [28] B. S. Simpkins, A. D. Dunkelberger, and I. Vurgaftman, *Chem. Rev.* **123**, 5020 (2023).
- [29] J. Yuen-Zhou and A. Koner, *J. Chem. Phys.* **160**, 154303 (2024).
- [30] M. Ruggenthaler, J. Flick, C. Pellegrini, H. Appel, I. V. Tokatly, and A. Rubio, *Phys. Rev. A* **90**, 012508 (2014).
- [31] J. Flick, H. Appel, M. Ruggenthaler, and A. Rubio, *J. Chem. Theory Comput.* **13**, 1616 (2017).
- [32] N. M. Hoffmann, H. Appel, A. Rubio, and N. T. Maitra, *Eur. Phys. J. B* **91**, 180 (2018).
- [33] X. Li, A. Mandal, and P. Huo, *J. Phys. Chem. Lett.* **12**, 6974 (2021).
- [34] M. A. D. Taylor, A. Mandal, W. Zhou, and P. Huo, *Phys. Rev. Lett.* **125**, 123602 (2020).
- [35] A. D. Wright, J. C. Nelson, and M. L. Weichman, *J. Am. Chem. Soc.* **145**, 5982 (2023).
- [36] A. D. Wright, J. C. Nelson, and M. L. Weichman, *J. Chem. Phys.* **159**, 164202 (2023).
- [37] T. E. Li, J. E. Subotnik, and A. Nitzan, *Proc. Natl. Acad. Sci. U.S.A.* **117**, 18324 (2020).
- [38] T. Szidarovszky, *Phys. Rev. A* **108**, 053118 (2023).
- [39] T. Szidarovszky, P. Badankó, G. J. Halász, and Á. Vibók, *J. Chem. Phys.* **154**, 064305 (2021).

Supplementary Information

Irén Simkó*

*Department of Chemistry, New York University, New York, New York 10003, USA and
Simons Center for Computational Physical Chemistry at New York University, New York, New York 10003, USA*

Norah M. Hoffmann†

*Department of Chemistry, New York University, New York, New York 10003, USA
Simons Center for Computational Physical Chemistry at New York University, New York, New York 10003, USA and
Department of Physics, New York University, New York, New York 10003, USA*

(Dated: March 26, 2025)

arXiv:2503.11968v2 [quant-ph] 25 Mar 2025

* is2873@nyu.edu

† norah.hoffmann@nyu.edu

I. MOLECULAR MODELS

A. HCl

For the *ab-initio* HCl molecule calculations we employ the following Morse potential energy curve:

$$V(R) = D_e(e^{-2\alpha(R-R_e)} - 2e^{-\alpha(R-R_e)} + 1), \quad (1)$$

where $R_e = 2.40855$ bohr is the equilibrium bond length, $D_e = 37209.369$ cm⁻¹ is the binding energy, and $\alpha = 0.993099$ bohr. The dipole moment curve is taken from Ref. [1], and the masses are $m(\text{H})=1837.1522$ a.u. and $m(\text{Cl})=63744.3019$ a.u..

B. 3-level system

In this 3-level model system the energies are given by $E_0 = 0$ a.u., $E_1 = 2 \cdot 10^{-1}$ a.u., $E_2 = 10 \cdot 10^{-1}$ a.u., assuming the populations of E_0 and E_1 are $p_0 = p_1 = 0.5$. The dipole matrix elements are $\mu_{02} = \mu_{20} = \mu_{12} = \mu_{21} = 1$ a.u. and $\mu_{ij} = 0$ otherwise. The linear susceptibility used for calculating the absorption spectrum in the fully classical model (see Eq. (5) of the main text) reads as [2]

$$\chi(\omega) = - \sum_{i < j} (p_i - p_j) \frac{Ng^2 |\mu_{ji}|^2}{\omega - E_i + E_j + i\gamma/2}, \quad (2)$$

with $g = \sqrt{\omega_c/(2\varepsilon_0 V)}$, where V is the cavity mode volume and $\gamma = 0.01$ a.u. is a damping coefficient. The spectrum on the bottom panel of Fig. 2(b) of the main text was obtained with $\kappa = 0.1$ a.u. as the photon escape parameter and $\sqrt{N}g = 0.2 \cdot 10^{-3}$ a.u. as the coupling strength parameter.

II. ADDITIONAL COMPUTATIONAL DETAILS

In the following, we provide a detailed discussion of the calculations for both the classical and quantum light models. It is important to note that in both cases, the material system is treated fully quantum mechanically, while only the treatment of light differs. The corresponding Hamiltonians can be found in Eqs. (1) and (4) of the main text. We only provide general expressions, assuming the rovibrational states of the molecule have been already computed. Detailed expressions for matrix elements with rovibrational states can be found, for example, in Ref. 3.

Additionally, in the fully quantum case, we consider two different approaches for computing observables: a static and a dynamic framework. This distinction allows for a direct comparison with classical observables. A key difference between the static quantum and time-dependent quantum (or classical) cavity models lies in the interpretation of polaritons. In the static framework, polaritons correspond to eigenstates of \hat{H} with hybrid light-matter character, where the degeneracy of a molecular excited state and a photonic excited state is lifted due to light-matter coupling. In contrast, in the time-dependent framework, polaritons emerge as dynamical features arising from periodic energy exchange between the molecule and the cavity light mode.

A. Quantum molecule - classical light mode model

In the classical light model, p and q are scalar variables. The initial conditions for the photonic vacuum state are $p(0) = q(0) = 0$ and the molecular initial state is an eigenstate of \hat{H}_{mol} , given by $|\Psi(0)\rangle = |\psi_i\rangle$. The time evolution of the light-matter system is governed by the following equations of motion:

$$|\dot{\Psi}(t)\rangle = -i \left(\hat{H}_{\text{mol}} + (g\sqrt{2\omega_c}q(t) + f(t))\hat{\mu}_Z + \frac{g^2}{\omega_c}\hat{\mu}_Z^2 \right) |\Psi(t)\rangle, \quad (3)$$

$$\dot{p}(t) = -\omega_c^2 q(t) - g\sqrt{2\omega_c} \langle \Psi(t) | \hat{\mu}_Z | \Psi(t) \rangle, \quad (4)$$

$$\dot{q}(t) = p(t), \quad (5)$$

where the cavity light mode is polarized in the laboratory-fixed Z direction and we apply a sharp but weak Gaussian pulse $f(t)$ as an initial kick to move the system out of equilibrium. The time-dependent molecular state is expressed in the basis of the cavity-free molecular eigenstates $|\psi_k\rangle$ with

$$|\Psi(t)\rangle = \sum_k C_{k,q}(t) e^{-iE_k t} |\psi_k\rangle, \quad (6)$$

where the subscript q indicates that the coefficients depend on the photonic state. The population of $|\psi_k\rangle$ is given by $p_k(t) = |C_{k,q}(t)|^2$. Substituting Eq. (6) in Eq. (3), we obtain the equations of motion expressed in terms of the $C_{k,q}(t)$ coefficients:

$$\dot{C}_{n,q}(t) = iE_n C_{n,q}(t) - i \sum_k C_{k,q}(t) e^{-i(E_k - E_n)t} \left(\langle \psi_n | \hat{H}_{\text{mol}} | \psi_k \rangle \right. \quad (7)$$

$$\left. + (g\sqrt{2\omega_c}q(t) + f(t)) \langle \psi_n | \hat{\mu}_Z | \psi_k \rangle + \frac{g^2}{\omega_c} \langle \psi_n | \hat{\mu}_Z^2 | \psi_k \rangle \right),$$

$$\dot{p}(t) = -\omega_c^2 q(t) - g\sqrt{2\omega_c} \mu_Z(t), \quad (8)$$

$$\dot{q}(t) = p(t), \quad (9)$$

where

$$\mu_Z(t) = \langle \Psi(t) | \hat{\mu}_Z | \Psi(t) \rangle = \sum_{k,k'} C_{k',q}^*(t) C_{k,q}(t) e^{-i(E_k - E_{k'})t} \langle \psi_{k'} | \hat{\mu}_Z | \psi_k \rangle, \quad (10)$$

is the time-dependent expectation value of the dipole moment. The matrix element of the $\hat{\mu}_Z^2$ is calculated as

$$\langle \psi_n | \hat{\mu}_Z^2 | \psi_{n'} \rangle = \sum_k \langle \psi_n | \hat{\mu}_Z | \psi_k \rangle \langle \psi_k | \hat{\mu}_Z | \psi_{n'} \rangle. \quad (11)$$

We obtain the absorption spectrum from the dipole autocorrelation function of $\mu_Z(t)$ and initial state $|\psi_i\rangle$ by

$$I_i(\omega) \propto \omega^2 \int_{-\infty}^{\infty} e^{-i\omega t} \langle \mu_Z(0) | \mu_Z(t) \rangle dt. \quad (12)$$

The total spectrum is calculated by summing the contributions of the different initial states with the appropriate Boltzmann weights:

$$I_{\text{tot}}(\omega) = \sum_i \exp\left(-\frac{E_i}{k_B T}\right) I_i(\omega). \quad (13)$$

B. Full quantum model

In the quantum case, \hat{q} and \hat{p} are expressed in terms of the creation \hat{a}^\dagger and annihilation \hat{a} operators,

$$\hat{q} = \sqrt{\frac{1}{2\omega_c}}(\hat{a}^\dagger + \hat{a}) \quad \text{and} \quad \hat{p} = i\sqrt{\frac{\omega_c}{2}}(\hat{a}^\dagger - \hat{a}). \quad (14)$$

Then, the dipole interaction term and the dipole self-energy are

$$\hat{V}_{\text{dip}} = g(\hat{a}^\dagger + \hat{a})\hat{\mu}_Z \quad \text{and} \quad \hat{V}_{\text{dse}} = \frac{g^2}{\omega_c}\hat{\mu}_Z^2, \quad (15)$$

respectively.

To obtain the polaritonic energies and eigenstates, we solve the time-independent Schrödinger-equation by diagonalizing the matrix of \hat{H} in the $|\psi_k, N\rangle = |\psi_k\rangle |N\rangle$ basis, where $|N\rangle$ denotes photon number states (Fock states). The matrix elements are given by

$$\langle \psi_{k'}, N' | \hat{H}_{\text{mol}} | \psi_k, N \rangle = \delta_{N', N} \delta_{k', k} E_k, \quad (16)$$

$$\langle \psi_{k'}, N' | \hat{H}_{\text{ph}} | \psi_k, N \rangle = \delta_{N', N} \delta_{k', k} N \omega_c, \quad (17)$$

$$\langle \psi_{k'}, N' | \hat{V}_{\text{dip}} | \psi_k, N \rangle = g \langle \psi_{k'}, N' | (\hat{a}^\dagger + \hat{a}) \hat{\mu}_Z | \psi_k, N \rangle = g(\sqrt{N+1} \delta_{N', N+1} + \sqrt{N} \delta_{N', N-1}) \langle \psi_{k'} | \hat{\mu}_Z | \psi_k \rangle, \quad (18)$$

$$\langle \psi_{k'}, N' | \hat{V}_{\text{dse}} | \psi_k, N \rangle = \frac{g^2}{\omega_c} \langle \psi_{k'}, N' | \hat{\mu}_Z^2 | \psi_k, N \rangle = \frac{g^2}{\omega_c} \delta_{N', N} \langle \psi_{k'} | \hat{\mu}_Z^2 | \psi_k \rangle. \quad (19)$$

1. Spectrum from the static framework

The eigenstates of \hat{H} expressed in the $|\psi_k, N\rangle$ basis are

$$|\Psi\rangle = \sum_k \sum_N C_{k, N} |\psi_k, N\rangle. \quad (20)$$

The absorption spectrum can be directly calculated from the polariton eigenstates, with the intensity of the transition between $|\Psi_i\rangle$ and $|\Psi_f\rangle$ given by

$$I(\Psi_i \rightarrow \Psi_f) = \frac{E_f^{\text{pol}} - E_i^{\text{pol}}}{hc} \exp\left(-\frac{E_i^{\text{pol}}}{k_B T}\right) \left(1 - \exp\left(-\frac{E_f^{\text{pol}} - E_i^{\text{pol}}}{k_B T}\right)\right) |\langle \Psi_i | \hat{\mu}_Z | \Psi_f \rangle|^2, \quad (21)$$

where E_i^{pol} and E_f^{pol} are the eigenenergies of the coupled light-matter Hamiltonian, corresponding to $|\Psi_i\rangle$ and $|\Psi_f\rangle$, respectively.

2. Spectrum from the time-dependent framework

Alternatively, the spectrum can be obtained using the time-dependent framework in the quantum model. This approach enables direct comparison with the classical light model. Here, we solve the time-dependent Schrödinger equation

$$i\dot{|\Psi(t)\rangle} = -i(\hat{H} + f(t)\hat{\mu}_Z) |\Psi(t)\rangle \quad (22)$$

where, as in the classical light model, a sharp but weak Gaussian pulse $f(t)$ is initially applied, and the initial condition is $|\Psi(0)\rangle = |\psi_i, 0\rangle$. The time-dependent wave function of the coupled light-matter system is expressed as

$$|\Psi(t)\rangle = \sum_k \sum_N C_{k,N}(t) e^{-i(E_k + N\omega_c)t} |\psi_k, N\rangle, \quad (23)$$

while the dipole moment is

$$\mu_Z(t) = \sum_N \sum_{k,k'} C_{k',N}^*(t) C_{k,N}(t) e^{-i(E_k - E_{k'})t} \langle \psi_{k'} | \hat{\mu}_Z | \psi_k \rangle. \quad (24)$$

The spectrum is then computed from $\mu_Z(t)$ through the dipole autocorrelation function according to Eqs. (12) and Eq. (13).

C. Factorized quantum model

For the factorized quantum model (discussion of Fig. 3(c) of the main text, dark purple dashed line), both the molecule and light are treated quantum mechanically, but the wave function is assumed to be the product of a molecular and photonic part: $|\Psi(t)\rangle = |\Psi_{\text{mol}}(t)\rangle |\Psi_{\text{ph}}(t)\rangle$. To compare with the quantum molecule-classical light model and the time-dependent full quantum framework, the spectrum is also calculated in the time-dependent framework here. The Hamiltonian, which includes a sharp Gaussian laser pulse, $f(t)$, at the beginning of the simulation, is partitioned into molecular, photonic, and dipole coupling terms:

$$\hat{H} = \hat{H}_{\text{mol+dse}} + \hat{H}_{\text{ph}} + \hat{V}_{\text{dip}}, \quad (25)$$

where the dipole self-energy and the laser pulse have been incorporated into $\hat{H}_{\text{mol+dse}}$:

$$\hat{H}_{\text{mol+dse}} = \hat{H}_{\text{mol}} + \frac{g^2}{\omega_c} \hat{\mu}_Z^2 + f(t) \hat{\mu}_Z. \quad (26)$$

The time-independent Schrödinger equation now reads

$$\begin{aligned} |\dot{\Psi}(t)\rangle &= |\dot{\Psi}_{\text{mol}}(t)\rangle |\Psi_{\text{ph}}(t)\rangle + |\Psi_{\text{mol}}(t)\rangle |\dot{\Psi}_{\text{ph}}(t)\rangle \\ &= -i \left((\hat{H}_{\text{mol+dse}} |\Psi_{\text{mol}}(t)\rangle) |\Psi_{\text{ph}}(t)\rangle + (\hat{H}_{\text{ph}} |\Psi_{\text{ph}}(t)\rangle) |\Psi_{\text{mol}}(t)\rangle + \hat{V}_{\text{dip}} |\Psi_{\text{mol}}(t)\rangle |\Psi_{\text{ph}}(t)\rangle \right). \end{aligned} \quad (27)$$

From this, we can obtain the following equations:

$$|\dot{\Psi}_{\text{mol}}(t)\rangle + \langle \Psi_{\text{ph}}(t) | \dot{\Psi}_{\text{ph}}(t) \rangle |\Psi_{\text{mol}}(t)\rangle = -i \left(\hat{H}_{\text{mol+dse}} + \langle \Psi_{\text{ph}}(t) | \hat{H}_{\text{ph}} | \Psi_{\text{ph}}(t) \rangle + \langle \Psi_{\text{ph}}(t) | \hat{V}_{\text{dip}} | \Psi_{\text{ph}}(t) \rangle \right) |\Psi_{\text{mol}}(t)\rangle \quad (28)$$

$$|\dot{\Psi}_{\text{ph}}(t)\rangle + \langle \Psi_{\text{mol}}(t) | \dot{\Psi}_{\text{mol}}(t) \rangle |\Psi_{\text{ph}}(t)\rangle = -i \left(\hat{H}_{\text{ph}} + \langle \Psi_{\text{mol}}(t) | \hat{H}_{\text{mol+dse}} | \Psi_{\text{mol}}(t) \rangle + \langle \Psi_{\text{mol}}(t) | \hat{V}_{\text{dip}} | \Psi_{\text{mol}}(t) \rangle \right) |\Psi_{\text{ph}}(t)\rangle \quad (29)$$

Since the coupling term, \hat{V}_{dip} is only a small perturbation, we take $\langle \Psi_{\text{ph}}(t) | \dot{\Psi}_{\text{ph}}(t) \rangle \approx -i \langle \Psi_{\text{ph}}(t) | \hat{H}_{\text{ph}} | \Psi_{\text{ph}}(t) \rangle$ and $\langle \Psi_{\text{mol}}(t) | \dot{\Psi}_{\text{mol}}(t) \rangle \approx -i \langle \Psi_{\text{mol}}(t) | \hat{H}_{\text{mol+dse}} | \Psi_{\text{mol}}(t) \rangle$. Substituting these into Eqs. (28) and (29) yields

$$|\dot{\Psi}_{\text{mol}}(t)\rangle = -i \left(\hat{H}_{\text{mol+dse}} + \langle \Psi_{\text{ph}}(t) | \hat{V}_{\text{dip}} | \Psi_{\text{ph}}(t) \rangle \right) |\Psi_{\text{mol}}(t)\rangle \quad (30)$$

$$|\dot{\Psi}_{\text{ph}}(t)\rangle = -i \left(\hat{H}_{\text{ph}} + \langle \Psi_{\text{mol}}(t) | \hat{V}_{\text{dip}} | \Psi_{\text{mol}}(t) \rangle \right) |\Psi_{\text{ph}}(t)\rangle. \quad (31)$$

Eqs. (30) and (31) are propagated starting from the $|\Psi_{\text{mol}}(0)\rangle = |\psi_i\rangle$, $|\Psi_{\text{ph}}(0)\rangle = |0\rangle$ initial condition, and the spectrum is obtained from the Fourier-transform of the dipole autocorrelation function.

D. Many-molecule models

The collective coupling is modeled by simulating N_{mol} identical molecules (in the gas phase) coupled to the cavity light mode. Cavity-free intermolecular interactions and spatial inhomogeneity effects (e.g., inhomogeneous electric field within the cavity) are neglected. The procedure for calculating the polariton states and absorption spectrum in the many-molecule case is the same as for the single-molecule case, except that the material wave function and the operators \hat{H}_{mol} and $\hat{\mu}_Z$ now correspond to N_{mol} molecules.

The collective polariton states involving N_{mol} molecules obey the Pauli permutation principle, meaning they must be symmetric or antisymmetric under odd permutations of identical bosonic or fermionic molecules, respectively [4]. Consequently, the basis functions used to express the collective states must exhibit the same symmetry properties. In the following, we construct appropriate molecular basis functions and matrix elements for the N_{mol} -molecule collective states and provide examples for $N_{\text{mol}} = 2$ in the case of a three-level system, while matrix elements for two diatomic molecules can be found in Ref. 5. The N_{mol} -molecule non-symmetrized basis functions are

$$|i_1 \dots i_{N_{\text{mol}}}\rangle = |i_1(1)\rangle \dots |i_{N_{\text{mol}}}(N_{\text{mol}})\rangle, \quad (32)$$

where $|i_k(k)\rangle$ denotes that the k th molecule is in the $|\psi_{i_k}\rangle$ state. From this, one can then construct the symmetry-adapted molecular basis states for bosonic molecules:

$$|i_1 \dots i_{N_{\text{mol}}}\rangle_B = \frac{1}{\tilde{N}} \sum_{\hat{R} \in S_{N_{\text{mol}}}} \hat{R} |i_1 \dots i_{N_{\text{mol}}}\rangle, \quad (33)$$

and for fermionic molecules:

$$|i_1 \dots i_{N_{\text{mol}}}\rangle_F = \frac{1}{\tilde{N}} \sum_{\hat{R} \in S_{N_{\text{mol}}}} p(\hat{R}) \hat{R} |i_1 \dots i_{N_{\text{mol}}}\rangle, \quad (34)$$

where \hat{R} are the permutation operators in the $S_{N_{\text{mol}}}$ symmetric group and $p(\hat{R}) = \pm 1$ for even/odd permutations, and \tilde{N} is a normalization factor. For example, for two 3-level system molecules the six bosonic basis states are

$$|ii\rangle_B = |ii\rangle = |\psi_i(1)\rangle |\psi_i(2)\rangle \quad \text{for } i \in \{0, 1, 2\} \quad (35)$$

$$|ij\rangle_B = \frac{1}{\sqrt{2}} (|ij\rangle + |ji\rangle) = \frac{1}{\sqrt{2}} (|\psi_i(1)\rangle |\psi_j(2)\rangle + |\psi_j(1)\rangle |\psi_i(2)\rangle) \quad \text{for } i \neq j \in \{0, 1, 2\}, \quad (36)$$

while the three fermionic basis states are

$$|ij\rangle_F = \frac{1}{\sqrt{2}} (|ij\rangle - |ji\rangle) = \frac{1}{\sqrt{2}} (|\psi_i(1)\rangle |\psi_j(2)\rangle - |\psi_j(1)\rangle |\psi_i(2)\rangle) \quad \text{for } i \neq j \in \{0, 1, 2\}. \quad (37)$$

In order to calculate the matrix elements of operator \hat{O} with the $|i_1 \dots i_{N_{\text{mol}}}\rangle_{B/F}$ basis states, we have to calculate terms of the form $\langle i'_1 \dots i'_{N_{\text{mol}}} | \hat{O} | i_1 \dots i_{N_{\text{mol}}} \rangle$. For the many-molecule molecular Hamiltonian, $\hat{H}_{\text{mol}} = \sum_{k=1}^{N_{\text{mol}}} \hat{H}_{\text{mol}}(k)$,

we obtain

$$\langle i'_1 \dots i'_{N_{\text{mol}}} | \hat{H}_{\text{mol}} | i_1 \dots i_{N_{\text{mol}}} \rangle = \left(\sum_{k=1}^{N_{\text{mol}}} E_{i_k} \right) \prod_{k=1}^{N_{\text{mol}}} \delta_{i'_k, i_k}. \quad (38)$$

The many-molecule dipole moment is approximated as the sum of the dipoles of the individual molecules, $\hat{\boldsymbol{\mu}} = \sum_{k=1}^{N_{\text{mol}}} \hat{\boldsymbol{\mu}}(k)$. In this case the matrix element is

$$\langle i'_1 \dots i'_{N_{\text{mol}}} | \hat{\boldsymbol{\mu}}_Z | i_1 \dots i_{N_{\text{mol}}} \rangle = \sum_{k=1}^{N_{\text{mol}}} \langle i'_k(k) | \hat{\boldsymbol{\mu}}_Z | i_k(k) \rangle \delta_{i'_1, i_1} \dots \delta_{i'_{k-1}, i_{k-1}} \delta_{i'_{k+1}, i_{k+1}} \delta_{i'_{N_{\text{mol}}}, i_{N_{\text{mol}}}}. \quad (39)$$

We now turn to the polariton absorption spectrum for two 3-level system molecules. The coupled light-matter states, obtained by diagonalizing the Hamiltonian in the product basis of the $|N=0\rangle$ and $|N=1\rangle$ Fock states and the collective molecular states from Eqs. (35-37), can be approximated by the states listed in Table I. For simplicity, each coupled state is approximated by the one or two basis states that dominate its eigenfunction. Nondegenerate polariton states, $|P_{k,\pm}\rangle_{B/F}$ (highlighted in bold), are formed when two basis states involving $|N=0\rangle$ and $|N=1\rangle$ have the same energy. The approximate splitting of the polariton states, $|P_{k,\pm}\rangle_{B/F} = (|ij\rangle_{B/F}|0\rangle \pm |i'j'\rangle_{B/F}|1\rangle)/\sqrt{2}$, denoted by Δ , can be calculated from the matrix element of \hat{V}_{dip} corresponding to the $|ij\rangle_{B/F}|0\rangle$ and $|i'j'\rangle_{B/F}|1\rangle$ basis functions,

$$\Delta \approx 2g_{(B/F)} \langle ij | \hat{\boldsymbol{\mu}}_Z | i'j' \rangle_{B/F} \langle 0 | (\hat{a}^\dagger + \hat{a}) | 1 \rangle = 2g_{(B/F)} \langle ij | \hat{\boldsymbol{\mu}}_Z | i'j' \rangle_{B/F}. \quad (40)$$

The \hat{V}_{dip} coupling matrix element, and therefore the corresponding splitting is not equal for all polariton states listed in Table I. The splitting of the $|P_{1,\pm}\rangle_B$ polariton states at $E \approx 10 \cdot 10^{-3}$ a.u. is

$$\Delta(|P_{1,\pm}\rangle_B) \approx \sqrt{2}g(\langle 20 | \hat{\boldsymbol{\mu}}_Z | 00 \rangle + \langle 02 | \hat{\boldsymbol{\mu}}_Z | 00 \rangle) = 2\sqrt{2}g\mu_0, \quad (41)$$

where $\mu_0 = \langle 0 | \hat{\boldsymbol{\mu}}_Z | 2 \rangle = \langle 1 | \hat{\boldsymbol{\mu}}_Z | 2 \rangle$, and we can similarly show that the splitting of the $|P_{3,\pm}\rangle_B$ polariton states at $E \approx 20 \cdot 10^{-3}$ a.u. is also $\Delta(|P_{3,\pm}\rangle_B) \approx 2\sqrt{2}g\mu_0$. On the other hand, the splitting of the $|P_{2,\pm}\rangle_B$ and $|P_{1,\pm}\rangle_F$ polaritons at $E \approx 12 \cdot 10^{-3}$ a.u. is smaller by a factor of $\sqrt{2}$:

$$\Delta(|P_{2,\pm}\rangle_B) \approx g(\langle 21 | \hat{\boldsymbol{\mu}}_Z | 01 \rangle + \langle 21 | \hat{\boldsymbol{\mu}}_Z | 10 \rangle + \langle 12 | \hat{\boldsymbol{\mu}}_Z | 01 \rangle + \langle 12 | \hat{\boldsymbol{\mu}}_Z | 10 \rangle) = 2g\mu_0 \quad (42)$$

and

$$\Delta(|P_{1,\pm}\rangle_F) \approx g(\langle 21 | \hat{\boldsymbol{\mu}}_Z | 01 \rangle - \langle 21 | \hat{\boldsymbol{\mu}}_Z | 10 \rangle - \langle 12 | \hat{\boldsymbol{\mu}}_Z | 01 \rangle + \langle 12 | \hat{\boldsymbol{\mu}}_Z | 10 \rangle) = 2g\mu_0. \quad (43)$$

The unequal splitting of the different polariton pairs manifests as broadened peaks in the spectrum, as we will show in the following.

In the fermionic case, only the $|01\rangle_F|0\rangle$ state is populated in thermal equilibrium, corresponding to one molecule in the $|\psi_0\rangle$ state and one in the $|\psi_1\rangle$ state. Each molecule can be excited to the $|\psi_2\rangle$ state, leading to two transitions:

- The R transition occurs when the molecule in $|\psi_0\rangle$ is excited to $|\psi_2\rangle$, corresponding to a transition to the polariton state, $|01\rangle_F|0\rangle \rightarrow |P_{1,\pm}\rangle_F$, which yields two peaks in the spectrum centered at $\omega \approx 10 \cdot 10^{-3}$ a.u. with a splitting of $\Delta(|P_{1,\pm}\rangle_F) \approx 2g\mu_0$ (Eq. (43)). This is the primary resonant polariton splitting.

- The P transition occurs when the molecule in $|\psi_1\rangle$ is excited to $|\psi_2\rangle$, corresponding to $|01\rangle_F |0\rangle \rightarrow |20\rangle_F |0\rangle$, resulting in a single peak at $\omega \approx 8 \cdot 10^{-3}$ a.u., meaning that the TP does not appear in the fermionic case.

In the bosonic case, the following three states are populated in thermal equilibrium: $|00\rangle_B |0\rangle$, $|01\rangle_B |0\rangle$, and $|11\rangle_B |0\rangle$. These correspond to the photonic ground state combined with (1) both molecules in $|\psi_0\rangle$, (2) one molecule in $|\psi_0\rangle$ and the other in $|\psi_1\rangle$, or (3) both molecules in the $|\psi_1\rangle$ state. Dipole transitions allow for exciting *exactly one* of the molecules to the $|\psi_2\rangle$ state, but not both, leading to the following transitions:

- A P transition at $\omega \approx 10 \cdot 10^{-3}$ a.u., corresponding to $|00\rangle_B |0\rangle \rightarrow |P_{1,\pm}\rangle_B$, occurs when one molecule is excited from $|\psi_0\rangle$ to $|\psi_2\rangle$ while the other remains in $|\psi_0\rangle$. This polariton transition is split, with a splitting of $\Delta(|P_{1,\pm}\rangle_B) \approx 2\sqrt{2}g\mu_0$ (see Eq. (41)).
- A P transition at $\omega \approx 10 \cdot 10^{-3}$ a.u., corresponding to $|01\rangle_B |0\rangle \rightarrow |P_{2,\pm}\rangle_B$, occurs when one molecule is excited from $|\psi_0\rangle$ to $|\psi_2\rangle$ while the other remains in $|\psi_1\rangle$. This polariton transition is also split, with a splitting of $\Delta(|P_{2,\pm}\rangle_B) \approx 2g\mu_0$ (see Eq. (42)).
- A R transition at $\omega \approx 8 \cdot 10^{-3}$ a.u., corresponding to $|01\rangle_B |0\rangle \rightarrow |P_{1,\pm}\rangle_B$, occurs when one molecule is excited from $|\psi_1\rangle$ to $|\psi_2\rangle$ while the other remains in $|\psi_0\rangle$. The splitting of this transition is $\Delta(|P_{1,\pm}\rangle_B) \approx 2\sqrt{2}g\mu_0$ (see Eq. (41)).
- A R transition at $\omega \approx 8 \cdot 10^{-3}$ a.u., corresponding to $|11\rangle_B |0\rangle \rightarrow |P_{2,\pm}\rangle_B$, occurs when one molecule is excited from $|\psi_1\rangle$ to $|\psi_2\rangle$ while the other remains in $|\psi_1\rangle$. The splitting of this transition is $\Delta(|P_{2,\pm}\rangle_B) \approx 2g\mu_0$ (see Eq. (42)).

This example shows that the TP splitting persists in the two-molecule case. However, the polariton side peaks become broadened because the splittings of the two P/R transitions are not equal: $2\sqrt{2}g\mu_0$ vs. $2g\mu_0$.

TABLE I. Approximate eigenstates of two noninteracting 3-level system molecules in a cavity. The light-matter basis states are denoted as $|ij\rangle_{B/F} |N\rangle$, where $|ij\rangle_{B/F}$ are the two molecule collective states in Eqs. (35-37), and $|N\rangle$ is a Fock state with $N = 0, 1$. Nondegenerate polariton states are noted in bold and labeled by $|P_{k,\pm}\rangle_{B/F}$.

Approx. $E/10^{-3}$ a.u.	Boson	Fermion
0.0	$ 00\rangle_B 0\rangle$	
2.0	$ 01\rangle_B 0\rangle$	$ 01\rangle_F 0\rangle$
4.0	$ 11\rangle_B 0\rangle$	
10.0	$ \mathbf{P}_{1,\pm}\rangle_B \equiv (20\rangle_B 0\rangle \pm 00\rangle_B 1\rangle)/\sqrt{2}$	$ 20\rangle_F 0\rangle$
12.0	$ \mathbf{P}_{2,\pm}\rangle_B \equiv (21\rangle_B 0\rangle \pm 01\rangle_B 1\rangle)/\sqrt{2}$	$ \mathbf{P}_{1,\pm}\rangle_F \equiv (21\rangle_F 0\rangle \pm 01\rangle_F 1\rangle)/\sqrt{2}$
14.0	$ 11\rangle_B 1\rangle$	
20.0	$ \mathbf{P}_{3,\pm}\rangle_B \equiv (22\rangle_B 0\rangle \pm 20\rangle_B 1\rangle)/\sqrt{2}$	$ 20\rangle_F 1\rangle$
22.0	$ 12\rangle_B 1\rangle$	$ 12\rangle_F 1\rangle$
30.0	$ 22\rangle_B 1\rangle$	

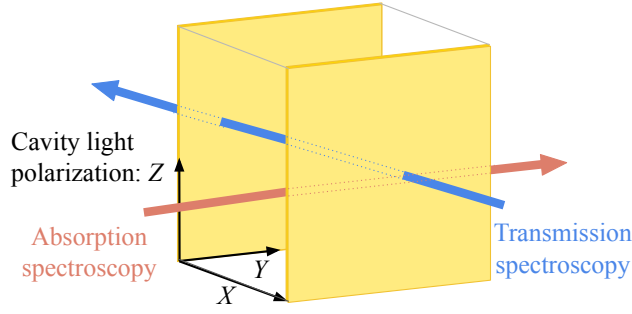


FIG. 1. Transmission and absorption spectroscopy for measuring polaritonic spectrum.

III. OPTIONS FOR POTENTIAL EXPERIMENTAL OBSERVATION OF THE TWIN-POLARITON SPLITTING

We hypothesize that the experimental observation of twin polariton splitting requires a setup different from current gas-phase polaritonic experiments employing transmission spectroscopy [6, 7]. In transmission spectroscopy, a probe laser is directed through the cavity perpendicular to the mirrors (e.g., along the X direction; see Fig. (1)), and the transmitted light intensity on the opposite side is measured. In this configuration, the laser can enter the cavity only if its frequency matches that of the cavity modes, i.e., $\omega = kc\pi/L$, where k is an integer and L is the length of the cavity [6, 7]. Consequently, if the cavity frequency is resonant with the R transition, a probe laser of the same frequency can enter the cavity, allowing the observation of primary polariton splitting. However, the twin-polariton splitting associated with the P transition cannot be observed in this setup since the P transition is not resonant with the cavity frequency, preventing the probe laser from entering the cavity. Hence, absorption spectroscopy might offer an alternative approach for observing the twin-polariton splitting. In this method, the probe laser is directed parallel to the mirrors (along the Y direction; see Fig. 1), thereby circumventing the restriction of cavity mode frequencies. With this in mind, we discuss the selection rules for polariton formation in the following section.

IV. SELECTION RULES FOR POLARITON FORMATION FOR THE HCL MOLECULE

In this section we discuss the selection rules governing polariton formation for a linear diatomic molecule and explain the origin of the remaining middle peak in the twin polariton splitting for HCl appearing in Fig. 1(b) of the main text. (Note that Ref. 5 also discusses these selection rules for a diatomic molecule.) In the rigid-rotor anharmonic oscillator model the molecular states are denoted as

$$|v, J, M\rangle = |v(R)\rangle \sqrt{(2J+1)/4\pi} D_{M,0}^{J*}(\theta, \phi), \quad (44)$$

where $|v(R)\rangle$ is the vibrational wave function corresponding to the v quantum number, R is the bond length, θ and ϕ are the polar and azimuthal angles describing the spatial orientation of the molecule, and $D_{M,K}^{J*}(\theta, \phi)$ are the Wigner D-matrices. Assuming that the cavity frequency is resonant with the $|v=0, J, M\rangle \rightarrow |v=1, J', M'\rangle$ transition, the $|v=0, J, M\rangle |N=1\rangle$ and $|v=1, J', M'\rangle |N=0\rangle$ light-matter basis states have equal energies and can

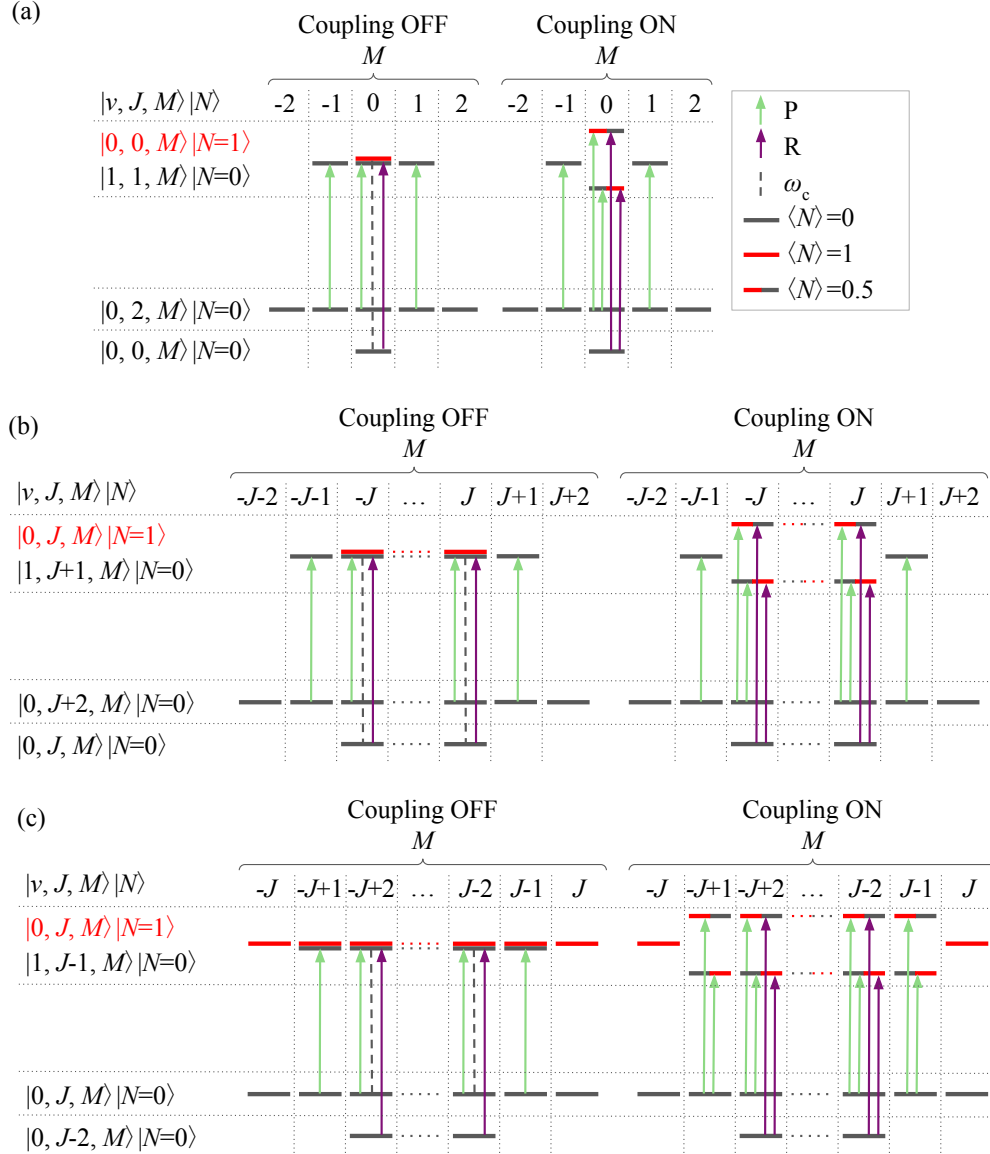


FIG. 2. Polariton formation and transitions in the polaritonic spectrum for a linear diatomic molecule. See Section IV for details. (a) Setup discussed for HCl in the main text: ω_c is resonant with $|v=0, J=0, M=0\rangle \rightarrow |v=1, J=1, M=0\rangle$ transition. The twin polariton peak (P) has a remaining middle peak. (b) General case, when ω_c is resonant with the $|v=0, J, M\rangle \rightarrow |v=1, J+1, M\rangle$ transition. There is a remaining middle twin polariton peak (P transition). (c) General case, when ω_c is resonant with the $|v=0, J, M\rangle \rightarrow |v=1, J-1, M\rangle$ transition. There is no remaining middle peak for either the primary (R) or the twin (P) polariton peaks.

couple. Assuming the cavity light mode is polarized in the Z direction, the matrix element of \hat{V}_{dip} (Eq. (15)) becomes

$$\begin{aligned}
 (\langle N=0 | \langle v=1, J', M' |) \hat{V}_{\text{dip}} (|v=0, J, M\rangle |N=1\rangle) &= g \langle 0 | \hat{a}^\dagger + \hat{a} | 1 \rangle \langle v=1, J', M' | \hat{\mu}_Z | v=0, J, M \rangle \\
 &= g \langle v=1, J', M' | \hat{\mu}_Z | v=0, J, M \rangle,
 \end{aligned} \tag{45}$$

where $\hat{\mu}_Z$ is the *space-fixed* Z component of the dipole moment, which depends on the *body-fixed* dipole moment $(\hat{\mu}_x, \hat{\mu}_y, \hat{\mu}_z)$ and the spatial orientation of the molecule. Following Ref.[8] we transform the space-fixed and body-

fixed dipole moment into spherical basis, $\hat{\mu}^{(1,\sigma)}$, where $\sigma = -1, 0, +1$:

$$\hat{\mu}_S^{(1,0)} = \hat{\mu}_Z, \quad \hat{\mu}_S^{(1,\pm 1)} = (\mp \hat{\mu}_X - i \hat{\mu}_Y) / \sqrt{2}, \quad (46)$$

$$\hat{\mu}_m^{(1,0)} = \hat{\mu}_z, \quad \hat{\mu}_m^{(1,\pm 1)} = (\mp \hat{\mu}_x - i \hat{\mu}_y) / \sqrt{2}, \quad (47)$$

where the subscripts S and m denote the space-fixed and body-fixed dipole, respectively. Next, we employ Wigner 3-D matrices to express the space-fixed dipole with the body-fixed dipole:

$$\hat{\mu}_S^{(1,\sigma)} = \sum_{\sigma'=-1}^1 D_{\sigma,\sigma'}^{1*} \hat{\mu}_m^{(1,\sigma')}. \quad (48)$$

In the case of a linear diatomic molecule, $\hat{\mu}_m^{(1,0)} = \hat{\mu}_z = \mu(R)$ and $\hat{\mu}_x = \hat{\mu}_y = 0$, therefore $\hat{\mu}_m^{(1,\pm 1)} = 0$. Substituting this into Eq. (48) gives

$$\hat{\mu}_Z = \hat{\mu}_S^{(1,0)} = D_{00}^{1*} \mu(R) = \cos(\theta) \mu(R) \quad (49)$$

and the coupling matrix element of \hat{V}_{dip} becomes

$$\begin{aligned} \langle \langle N = 0 | \langle v = 1, J', M' | \rangle \hat{V}_{\text{dip}} | v = 0, J, M \rangle | N = 1 \rangle \rangle &= g \langle v = 1, J', M' | \hat{\mu}_Z | v = 0, J, M \rangle \\ &= g \langle v = 1 | \mu(R) | v = 0 \rangle \langle J', M' | D_{00}^{1*} | J, M \rangle \\ &= g \mu_{01} \frac{(2J+1)(2J'+1)}{4\pi} (-1)^M \begin{pmatrix} J' & 1 & J \\ 0 & 0 & 0 \end{pmatrix} \begin{pmatrix} J' & 1 & J \\ M' & 0 & -M \end{pmatrix}, \end{aligned} \quad (50)$$

where $\mu_{01} = \langle v = 1 | \mu(R) | v = 0 \rangle$, ($:::$) are the Wigner 3J-symbols and we used

$$\langle J', K', M' | D_{mk}^{j*} | J, K, M \rangle = \sqrt{(2J+1)(2J'+1)} (-1)^{m-k+M-K} \begin{pmatrix} J' & j & J \\ K' & -k & -K \end{pmatrix} \begin{pmatrix} J' & j & J \\ M' & -m & -M \end{pmatrix}. \quad (51)$$

Eq. (50) yields the selection rules of polariton formation, i.e., which combinations of $|v = 0, J, M \rangle |N = 1 \rangle$ and the $|v = 1, J', M' \rangle |N = 0 \rangle$ can couple. Due to the properties of the Wigner 3J-symbols, the coupling matrix element in Eq. (50) can be nonzero only if $J' = J \pm 1$ and $M' = M$. Therefore, the possible polariton states are

$$|P_{J+1,\pm} \rangle \approx (|v = 0, J, M \rangle |N = 1 \rangle \pm |v = 1, J+1, M \rangle |N = 0 \rangle) / \sqrt{2}, \quad (52)$$

$$|P_{J-1,\pm} \rangle \approx (|v = 0, J, M \rangle |N = 1 \rangle \pm |v = 1, J-1, M \rangle |N = 0 \rangle) / \sqrt{2}. \quad (53)$$

The next question to consider is how these polariton states appear in an absorption spectroscopy measurement (see Section III), where we assume that the probe laser is polarized in the space-fixed Z direction. The intensity of the $|v = 0, J^*, M^* \rangle |N = 0 \rangle \rightarrow |P_{J\pm 1,\pm} \rangle$ transitions is determined by the transition dipole moment

$$I \propto |\langle \langle N = 0 | \langle v = 0, J^*, M^* | \rangle \hat{\mu}_Z | P_{J\pm 1,\pm} \rangle \rangle|^2 = \frac{1}{2} |\langle v = 0, J^*, M^* | \hat{\mu}_Z | v = 1, J \pm 1, M \rangle|^2, \quad (54)$$

since only the $N = 0$ (“material excited state”) part of the polariton states contributes to the intensity. It is straightforward to show that the intensity can be nonzero if $M^* = M$ and $J^* = J$ or $J+2/J-2$ for $|P_{J+1,\pm} \rangle / |P_{J-1,\pm} \rangle$.

Now let us discuss how the selection rules apply to the setup described in the main text and how this leads to the remaining middle peak of the twin polariton for the HCl molecule (see Fig. 2(a) here and Fig. 1(b-c) of the main text).

In this setup, the cavity frequency is resonant with the $|v = 0, J = 0, M = 0\rangle \rightarrow |v = 1, J' = 1, M' = 0\rangle$ transition of the HCl molecule. The $|v = 0, J = 0, M = 0\rangle |N = 1\rangle$ and $|v = 1, J' = 1, M' = 0\rangle |N = 0\rangle$ states are degenerate (see Fig. 2(a), “Coupling OFF”), and when they hybridize, they give rise to the two polariton states

$$|P_{\pm}\rangle \approx (|v = 0, J = 0, M = 0\rangle |N = 1\rangle \pm |v = 1, J' = 1, M' = 0\rangle |N = 0\rangle) / \sqrt{2}, \quad (55)$$

whose energy degeneracy is lifted (see Fig. 2(a), “Coupling ON”). However, the $|v = 1, J' = 1, M' = \pm 1\rangle |N = 0\rangle$ states also have the same energy as the $|v = 0, J = 0, M = 0\rangle |N = 1\rangle$ state, but cannot couple with it as $M' = M$ is not satisfied. This means that the $|v = 1, J = 1', M' = \pm 1\rangle |N = 0\rangle$ states cannot form light-matter hybridized states and their energy is the same as in the absence of light-matter coupling (see Fig. 2(a), “Coupling ON”). Note that OFF/ON means in cavity but with and without light-matter coupling.

In the polariton spectrum, the primary polariton splitting (R peak) corresponds to $|v = 0, J = 0, M = 0\rangle |N = 0\rangle \rightarrow |P_{\pm}\rangle$, while the side peaks of the twin-polariton splitting (P peak) correspond to $|v = 0, J = 2, M = 0\rangle |N = 0\rangle \rightarrow |P_{\pm}\rangle$, according to the selection rules. The remaining middle peak of the twin-polariton peak is due to the $|v = 0, J = 2, M = \pm 1\rangle |N = 0\rangle \rightarrow |v = 1, J' = 1, M' = \pm 1\rangle |N = 0\rangle$ transition, whose frequency is the same as that of the cavity-free transition.

As shown in Fig. 2(b), if the cavity frequency is resonant with the $|v = 0, J, M\rangle \rightarrow |v = 0, J + 1, M\rangle$ transition, then the $(|v = 0, J, M\rangle |N = 1\rangle$ and $|v = 1, J + 1, M\rangle |N = 0\rangle)$ states can hybridize if $-J \leq M \leq J$, and form the $|P_{J+1,\pm}\rangle$ polariton states (Eq. (52)). The $|v = 0, J, M\rangle \rightarrow |P_{J+1,\pm}\rangle$ transitions yield the primary polariton splitting (R), while $|v = 0, J + 2, M\rangle \rightarrow |P_{J+1,\pm}\rangle$ yields the twin-polariton splitting (P). The $|v = 1, J + 1, M' = \pm(J + 1)\rangle |N = 0\rangle$ states cannot hybridize with any $|v = 0, J, M\rangle |N = 1\rangle$ state because of the $M' = M$ selection rule, therefore, the $|v = 0, J + 2, M = \pm(J + 1)\rangle |N = 0\rangle \rightarrow |v = 1, J + 1, M' = \pm(J + 1)\rangle |N = 0\rangle$ transitions give rise to the remaining middle peak in the twin-polariton splitting. If the cavity frequency is resonant with the $|v = 0, J, M\rangle \rightarrow |v = 0, J - 1, M\rangle$ transition, the spectrum will be different, as there will be no remaining middle peak in twin-polariton splitting (see Fig. 2(c)). The $(|v = 0, J, M\rangle |N = 1\rangle$ and $|v = 1, J - 1, M\rangle |N = 0\rangle)$ states hybridize if $-J + 1 \leq M \leq J - 1$ and form the $|P_{J-1,\pm}\rangle$ polariton states (Eq. (53)). In the spectrum, the primary and twin-polariton splittings correspond to the $|v = 0, J, M\rangle \rightarrow |P_{J-1,\pm}\rangle$ and $|v = 0, J - 2, M\rangle \rightarrow |P_{J-1,\pm}\rangle$ transitions, respectively, with $-J + 1 \leq M \leq J - 1$ in both cases. There will be no remaining middle peak for either the twin- or the primary resonant polariton peaks, because even though the $|v = 0, J, M = \pm J\rangle |N = 1\rangle$ states cannot hybridize with any $|v = 1, J - 1, M'\rangle |N = 0\rangle$, transitions into this state are not visible in the spectrum as it is an excited photonic state.

-
- [1] G. Maroulis, *Mol. Phys.* **74**, 131 (1991).
 - [2] J. Yuen-Zhou and A. Koner, *J. Chem. Phys.* **160**, 154303 (2024).
 - [3] T. Szidarovszky, *J. Chem. Phys.* **159**, 014112 (2023).
 - [4] T. Szidarovszky, *Phys. Rev. A* **108**, 053118 (2023).
 - [5] T. Szidarovszky, *J. Chem. Phys.* **162**, 034117 (2025).
 - [6] A. D. Wright, J. C. Nelson, and M. L. Weichman, *J. Am. Chem. Soc.* **145**, 5982 (2023).
 - [7] A. D. Wright, J. C. Nelson, and M. L. Weichman, *J. Chem. Phys.* **159**, 164202 (2023).
 - [8] P. R. Bunker and P. Jensen, *Molecular symmetry and spectroscopy*, Vol. 46853 (NRC research press, 2006).